Dynamics of two interacting hydrogen bubbles in liquid aluminum under the influence of a strong acoustic field

Gerard S. B. Lebon[*] and Koulis Pericleous

Centre for Numerical Modelling and Process Analysis, The University of Greenwich, London, SE10 9LS, United Kingdom

Iakovos Tzanakis and Dmitry G. Eskin

Brunel Centre for Advanced Solidification Technology, Brunel University, Uxbridge, Middlesex, UB8 3PH, United Kingdom

Ultrasonic melt processing significantly improves the properties of metallic materials. However, this promising technology has not been successfully transferred to the industry because of difficulties in treating large volumes of melt. To circumvent these difficulties, a fundamental understanding of the efficiency of ultrasonic treatment of liquid metals is required. In this endeavor, the dynamics of two interacting hydrogen bubbles in liquid aluminum are studied to determine the effect of a strong acoustic field on their behavior. It is shown that coalescence readily occurs at low frequencies in the range of 16 to 20 kHz; forcing frequencies at these values are likely to promote degassing. Emitted acoustic pressures from relatively isolated bubbles that resonate with the driving frequency are in the megapascal range and these cavitation shock waves are presumed to promote grain refinement by disrupting the growth of the solidification front.

I. INTRODUCTION

Treating liquid metals near their liquidus temperature with ultrasound is known to significantly improve the functional quality and properties of the processed metallic materials [1–4]: beneficial effects of the ultrasonic treatment include degassing of dissolved gases, improved wetting and/or the activation of inclusions by cleaning the solid-liquid interface, enhancing nucleation, and refining the grain structure of the solidified sample [1,5]. These improvements are attributed to acoustic cavitation [6]. However, the treatment of large volumes of liquid metal, as is required by industrial processes like continuous casting, is still elusive: the process is time consuming and can currently be applied only to a fixed volume of melt in a crucible. To circumvent these difficulties and facilitate the transfer of this promising technology to the industry, a fundamental understanding of gas bubble behavior in the sonicated melt is required [7].

Homogeneous cavitation models have been used by different authors [8–10] to predict the cavitation regions in a liquid melt with reasonable success. However, these Eulerian models do not take into account the mutual interaction of the cavitating bubbles, due to a phenomenon commonly expressed through the Bjerknes forces [11]. Mutual interaction affects coalescence, formation of bubble streamers and clouds, and shielding of the sonotrode source. Therefore, a more complete understanding of ultrasonic treatment in liquid metal processing and of the different bubble structures observed by x-ray tomography [12] and radiography [13,14] in aluminum alloys requires the modeling of bubble interaction.

The dynamics of interacting bubbles in strong acoustic fields have been previously investigated in water, in an attempt to explain the formation of stable streamers [15,16]. Mettin *et al.* [17] have studied the mutual interaction of small oscillating cavitating bubbles numerically. Their results

showed that the strengths and directions of secondary Bjerknes forces on each interacting bubble differed greatly from the classical linear theory. Pelekasis *et al.* [18] studied the motion of two interacting bubbles to explain the formation of stable bubble clusters in intense acoustic fields. Jiang *et al.* [19] reported the frequency spectrum from the pressure emitted by two interacting bubbles in the presence of a strong acoustic field and demonstrated that the interaction between bubbles adds a nonlinear effect on their oscillation. Doinikov [20] used the Lagrangian formalism to calculate the translational motion of the two interacting bubbles directly: this formulation will be used in this paper to understand the dynamics of hydrogen bubbles in a liquid aluminium melt under ultrasonic treatment.

While cavitation is not necessary for degassing in water [21], the efficiency of ultrasonic degassing in light alloys melts has been found to be a function of cavitation development [1]. A study of the dynamics of interacting hydrogen bubbles can also shed light on the coalescence stage of the degassing process in liquid melts. Ultrasonic degassing in liquid metals consists of these three stages [1,21]: (1) cavitation nuclei seed gas bubbles, which grow in the oscillating ultrasonic field through rectified diffusion, (2) bubbles coalesce due to Bjerknes and Bernoulli forces, and (3) they finally float to the surface due to buoyancy.

Hydrogen is chosen as it is the main gas dissolved in liquid aluminum. The vapor pressure of aluminum at its melting point is 0.000012 Pa [22], and therefore vapor bubbles are unlikely to form in the liquid bulk [23]. Cavitation is thus mainly attributed to both the hydrogen-containing inclusions and the dissolved hydrogen that is released from aluminum when the local pressure decreases [1].

Because the distance between stable cavitating bubbles is large compared with their radii [12], bubble shape distortions are ignored and this paper concentrates solely on the radial motion and translational motion of bubble centers. This is particularly true for hydrogen bubbles in liquid aluminum: they tend to stay spherical [12] due to the large interfacial tension between hydrogen and liquid aluminum [1].

---

[*]G.S.B.Lebon@greenwich.ac.uk

II. THEORY

The equations of radial and translational motions of two spherical interacting bubbles, schematically shown in Fig. 1, in a strong acoustic field have been derived by Doinikov [20] as

$$\left(1 - \frac{\dot{R}_1}{c}\right) R_1 \ddot{R}_1 + \left(\frac{3}{2} - \frac{\dot{R}_1}{2c}\right) \dot{R}_1^2 - \frac{1}{\rho}\left(1 + \frac{\dot{R}_1}{c}\right) p_1 - \frac{R_1}{\rho c}\frac{dp_1}{dt}$$

$$= \frac{\dot{x}_1^2}{4} - \frac{R_2^2 \ddot{R}_2 + 2 R_2 \dot{R}_2^2}{D} + \frac{R_2^2(\dot{x}_1 \dot{R}_2 + R_2 \ddot{x}_2 + 5\dot{R}_2 \dot{x}_2)}{2D^2} - \frac{R_2^3 \dot{x}_2(\dot{x}_1 + 2\dot{x}_2)}{2D^3}, \tag{1}$$

$$\left(1 - \frac{\dot{R}_2}{c}\right) R_2 \ddot{R}_2 + \left(\frac{3}{2} - \frac{\dot{R}_2}{2c}\right) \dot{R}_2^2 - \frac{1}{\rho}\left(1 + \frac{\dot{R}_2}{c}\right) p_2 - \frac{R_2}{\rho c}\frac{dp_2}{dt} = \frac{\dot{x}_2^2}{4} - \frac{R_1^2 \ddot{R}_1 + 2 R_1 \dot{R}_1^2}{D}$$

$$+ \frac{R_1^2(\dot{x}_2 \dot{R}_1 + R_1 \ddot{x}_1 + 5\dot{R}_1 \dot{x}_1)}{2D^2} - \frac{R_1^3 \dot{x}_1(\dot{x}_2 + 2\dot{x}_1)}{2D^3}, \tag{2}$$

$$\frac{R_1 \ddot{x}_1}{3} + \dot{R}_1 \dot{x}_1 + \frac{1}{D^2}\frac{d}{dt}\left(R_1 R_2^2 \dot{R}_2\right) - \frac{R_2^2(R_1 R_2 \ddot{x}_2 + R_2 \dot{R}_1 \dot{x}_2 + 5 R_1 \dot{R}_2 \dot{x}_2)}{D^3} = \frac{F_{\text{ex},1}}{2\pi\rho R_1^2}, \tag{3}$$

$$\frac{R_2 \ddot{x}_2}{3} + \dot{R}_2 \dot{x}_2 + \frac{1}{D^2}\frac{d}{dt}\left(R_2 R_1^2 \dot{R}_1\right) - \frac{R_1^2(R_1 R_2 \ddot{x}_1 + R_1 \dot{R}_2 \dot{x}_1 + 5 R_2 \dot{R}_1 \dot{x}_1)}{D^3} = \frac{F_{\text{ex},2}}{2\pi\rho R_2^2}, \tag{4}$$

where R_i, $\dot{R}_i$, and $\ddot{R}_i$ are the radius, radial velocity, and radial acceleration of bubble i, respectively. x_i, $\dot{x}_i$, and $\ddot{x}_i$ are the position, velocity, and acceleration of the center of bubble i, respectively. c is the speed of sound in the liquid. ρ is the density of liquid. $D = x_2 - x_1$ is the distance between the bubble centers. Equations (1) and (2) define the radial motion of bubbles 1 and 2, respectively, and are based on the Keller-Miksis model [24], which is adequate for large external amplitudes and accounts for the acoustic radiation from each bubble. Equations (3) and (4) define the translational motion of bubbles 1 and 2, respectively.

The pressures p_i are given by

$$p_i = P_{g_{i,0}}\left(\frac{R_{i0}}{R_i}\right)^{3\kappa} + p_v - \frac{2\sigma}{R_i} - \frac{4\mu\dot{R}_i}{R_i}$$

$$- P_0 - \rho g h_i + P_a \sin(2\pi f t), \tag{5}$$

where the initial gas pressure in bubble i is $P_{g_{i,0}} = P_0 + p_v + \rho g h_i + 2\sigma/R_{i0}$. P_0 is the atmospheric pressure and is equal to 1 bar, κ is the polytropic exponent, p_v is the vapor pressure of the liquid, g is the gravitational acceleration, h_i is the depth of bubble i below the liquid free surface, σ is the surface tension between the liquid and bubble gas, R_{i0} and $\dot{R}_{i0}$ are the initial radius and radial velocity for bubble i, μ is the dynamic viscosity of the liquid, P_a is the amplitude of the external pressure field, and f is the frequency of the external field. While the pressure term $\rho g h_i$ may be less important in water, it cannot be ignored for denser liquids like aluminum.
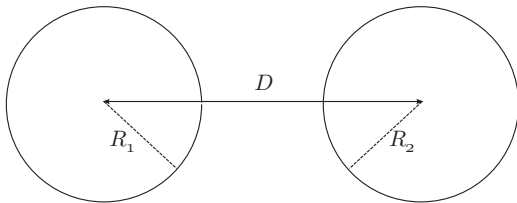

FIG. 1. Geometry of interacting bubbles. Coalescence occurs when $D < R_1 + R_2$.

Prosperetti demonstrated that the effective polytropic exponent κ is strongly dependent on the driving frequency [25]. Zhang rederived an expression for the polytropic exponent that is applicable to forcing signals of large frequencies and simplified it as [26]

$$\kappa = \tfrac{1}{3}\text{Re}(\Phi), \tag{6}$$

Φ is given by

$$\Phi = \frac{3\gamma}{1 - 3(\gamma - 1)i\chi[(i/\chi)^{1/2}\coth(i/\chi)^{1/2} - 1]}, \tag{7}$$

where

$$\chi = D_{g,p}/(2\pi f R_0^2). \tag{8}$$

$D_{g,p}$ is the thermal diffusivity of the gas at constant pressure. R_0 is the equilibrium radius of the gas bubble. $\gamma = 1.4054$ is the ratio of specific heat capacities for hydrogen. Equation (7) is valid only when $G_1 G_2 \ll 1$, a condition that is met in most practical situations, where

$$G_1 = 2\pi M_g D_{g,p} f/(R_g T_\infty), \tag{9}$$

$$G_2 = 1/(\gamma\chi). \tag{10}$$

M_g is the molecular weight of the gas bubble, R_g is the universal gas constant, and T_∞ is the temperature of the liquid far from the bubble.

The external forces $F_{\text{ex},i}$ exerted on bubble i are equal to the Levich viscous drag [27] and are given by

$$F_{\text{ex},i} = -12\pi\mu R_i(\dot{x}_i - v_{3-i}), \tag{11}$$

where v_i is the liquid velocity generated by the ith bubble at the center of the other bubble. This velocity is expanded to

$$v_i = -\frac{(-1)^{-1} R_i^2 \dot{R}_i}{D^2} + \frac{R_i^3 \dot{x}_i}{D^3}, \tag{12}$$

up to the order D^{-3}.

The resonant frequency f_{i0} of a bubble i with an equilibrium radius R_{io} is given by the Minnaert relationship [28]:

$$f_{i0} = \frac{1}{2\pi R_{i0}} \sqrt{\frac{1}{\rho} \left[3\kappa p_{g_{i,0}} - \frac{2\sigma}{R_{i0}} \right]} \qquad (13)$$

III. RESULTS AND DISCUSSIONS

A. Frequency dependence of coalescence

Two hydrogen bubbles in liquid aluminum at $T_\infty = 700\,^\circ\text{C}$ and subjected to an external field with frequency in the range $16\,\text{kHz} \leqslant f \leqslant 30\,\text{kHz}$ are considered. The material properties for liquid aluminum are $\rho = 2375\,\text{kgm}^{-3}$, $\sigma = 0.860\,\text{Nm}^{-1}$, $\mu = 0.001\,\text{kgm}^{-1}\text{s}^{-1}$, $p_v = 0.000012\,\text{Pa}$ corresponding to the minute presence of aluminum vapor in the bubble, $c = 4600\,\text{ms}^{-1}$, $D_{g,p} = 1.7 \times 10^{-4}\,\text{m}^2\text{s}^{-1}$, and κ is calculated using Eq. (6) since $G_1 G_2 \ll 1$ for the range of frequencies and radii considered in this study. These conditions are commonly met by experimental setups for which measured acoustic pressures and frequency spectra are available [29].

The variation of resonant frequency with bubble radius for the range $1\,\mu\text{m} < R_{i0} < 1\,\text{mm}$ is shown in Fig. 2. Resonant frequencies for this range of bubble radii is covered by the bandwidth of the calibrated cavitometer used in this study [30]. Note that assuming adiabatic bubble oscillations ($\kappa = \gamma$) leads to an over-estimation of the resonant frequency for radii larger than 10 μm, as shown by the dotted line; however, the adiabatic approximation is valid for bubbles of radii smaller than 10 μm. The resonant frequency of bubbles is also independent of the forcing frequency value when $R_{i0} < 10\,\mu\text{m}$.

The system of Eqs. (1), (2), (3), and (4) is solved in the software package Wolfram Mathematica 10 [31] for 150 acoustic cycles, with $R_{10} = R_{20}$ set to vary within the above radius range. Longer runs (300 cycles) in the 17.7 kHz set did not reveal the occurrence of additional coalescence and the number of cycles was limited to 150 for all other frequencies to reduce the run time of the solver. The initial distances $D[t = 0]$ considered in this study are in the range 0.1 to 2.0 mm, corresponding to typical separation distances for oscillating
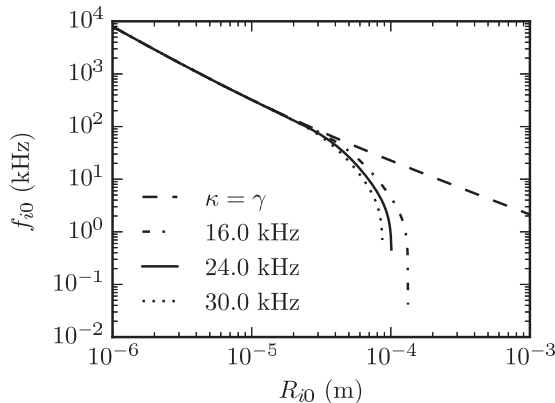

FIG. 2. Resonant frequencies for hydrogen bubbles of different radii in liquid aluminum. The dotted line shows the resonant frequency variation at a forcing frequency f of 16.0 kHz using the adiabatic condition $\kappa = \gamma$.

bubbles [12,17]. Figure 3 shows the number of cycles taken for coalescence to occur (when $D < R_1 + R_2$).

In the frequency range $16\,\text{kHz} \leqslant f \leqslant 20\,\text{kHz}$ [Figs. 3(a)–3(c)], coalescence readily occurs for all bubbles with initial separation less than 2 mm, indicating the existence of a strong attractive force between these bubbles. Coalescence takes more time, of the order of 20 acoustic cycles, for bubbles of initial separation of 2 mm and initial radii of 100 μm. These bubbles, with initial resonant frequencies of 3.8 kHz, are less responsive to the effect of the forcing signal of the sonotrode.

Larger frequencies [Figs. 3(d)–3(f)] offer larger coalescence times compared with the previous frequency range. While the behavior at the smallest initial distance (0.7 mm) or less is identical, larger separations lead to much slower coalescence rates. Therefore, forcing frequencies lower than 20 kHz are expected to be more efficient for coalescing bubbles and increasing the degassing rate of hydrogen bubbles from the aluminum melt.

B. Acoustic spectra at $f = 17.7\,\text{kHz}$

The experimentally measured frequency emissions from a treated volume of aluminum are shown in Fig. 4. 5.2 kg of aluminum, corresponding to 2 L of melt, was melted and heated in a clay-graphite crucible of diameter 15 cm. A 20-mm preheated sonotrode was immersed at a depth $h = 20\,\text{mm}$ below the free surface. The melt was treated with ultrasound at a power of 3.5 kW, corresponding to a pressure of 1.0 MPa below the radiating horn [32] and a forcing frequency of 17.7 kHz. The frequency emissions have been measured with a calibrated cavitometer [30] with the tip immersed 5 cm below the horn [Fig. 4(a)] and outside the crucible with an ultrasound microphone [Fig. 4(b)]. The ultrasonic microphone has a sampling rate of 250 K per second and a frequency range up to 125 kHz [33].

Based on these frequency measurements, the radii that are listed in Table I are of interest. The subharmonic (8.9 kHz), forcing frequency (17.7 kHz), and first ultraharmonic (26.6 kHz) are the prominent low-frequency peaks as measured by both the cavitometer and the microphone. Bubbles of radii 80, 64, and 54 μm are associated with these low frequencies. The hump from 190 to 400 kHz in the cavitometer probe measurement indicates another region of activity. Two representative bubbles of 15 and 8.4 μm are studied to reflect this frequency range. Finally, the largest noticeable peak of 1.04 MHz is generally attributed to stable cavitating bubbles at low forcing pressures and contribute to

TABLE I. Resonant frequencies, associated bubble radii, and Reynolds number for flows due to bubble radial oscillations.

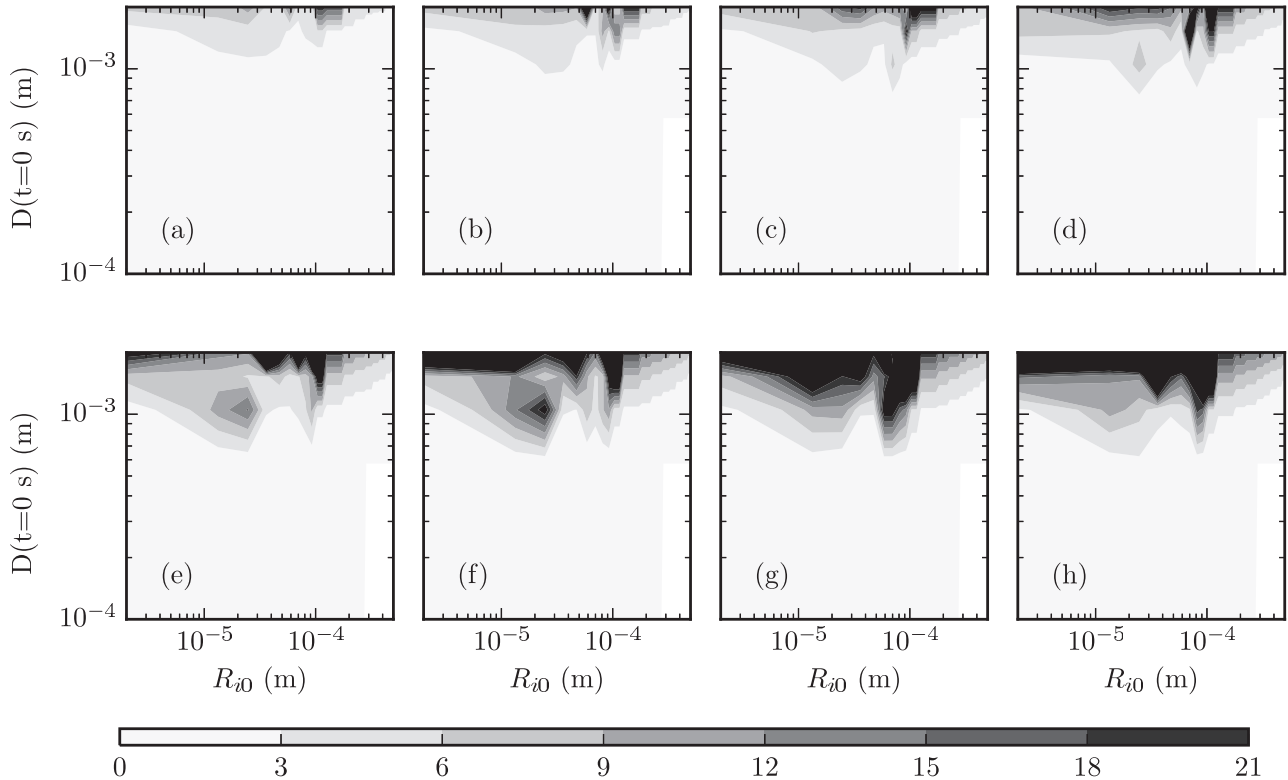| Resonant frequency f_{i0} kHz	Resonant bubble radius R_{i0} μm	Reynolds number Re
8.9	80	850
17.7	64	1100
26.6	55	1200
190	15	670
400	8.4	420
1040	4.1	260

FIG. 3. Coalescence maps for $P_a = 1.0$ MPa for different sonotrode frequencies f: (a) $f = 16.0$ kHz, (b) $f = 18.0$ kHz, (c) $f = 20.0$ kHz, (d) $f = 22.0$ kHz, (e) $f = 24.0$ kHz, (f) $f = 26.0$ kHz, (g) $f = 28.0$ kHz, (h) $f = 30.0$ kHz. The contours represent the number of acoustic cycles after which coalescence is achieved.

the cavitation broadband noise. This corresponds to bubbles of radius 4.1 μm. The Reynolds number of flow considering the radial oscillations is given by $\text{Re} = 2\pi\rho R_i^2 f_i / \mu$. Flow around the bubbles is well into the laminar regime.

With an initial separation of 1 mm, the bubbles coalesce rapidly, within a few acoustic cyles as shown in Fig. 5. Coalescence leads to larger, lower-frequency bubbles, which will leave the domain through buoyancy: together with rectified diffusion—the gradual increase in gas content inside the bubble as it pulsates—this is a phenomenon leading to ultrasonic degassing [1]. This effect is particularly fast for large

bubbles, where coalescence is achieved within a few acoustic cycles. The initial separation between bubbles is, therefore, an essential parameter that determines whether the hydrogen bubbles are likely to survive on their own or coalesce.

The same behavior is observed with larger separations of 2 mm as shown in Fig. 6. However, bubbles of initial radii in resonance in sub- and ultraharmonics survive for longer, while bubbles whose resonant frequency matches the forcing frequency of the sonotrode coalesce much faster [Fig. 6(b)]. With these observations, it appears the use of a particular forcing frequency may affect the optimization of the process,
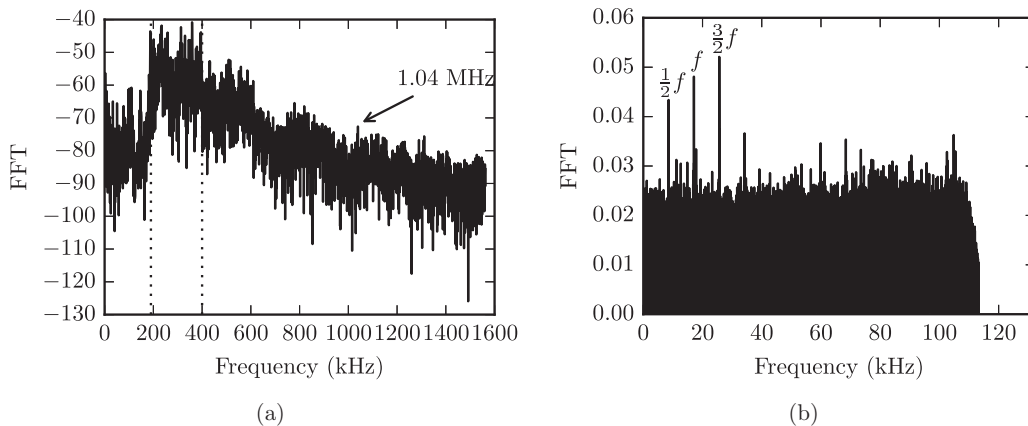

FIG. 4. Frequency spectra measured in the aluminum crucible experiment. (a) Cavitometer probe frequency response when placed 5 cm below the sonotrode axis. The two dotted lines represent the frequency boundaries of the hump in the cavitometer response (190–400 kHz). The largest peak in the MHz region is annotated. (b) Frequency response from the external ultrasonic microphone recording.
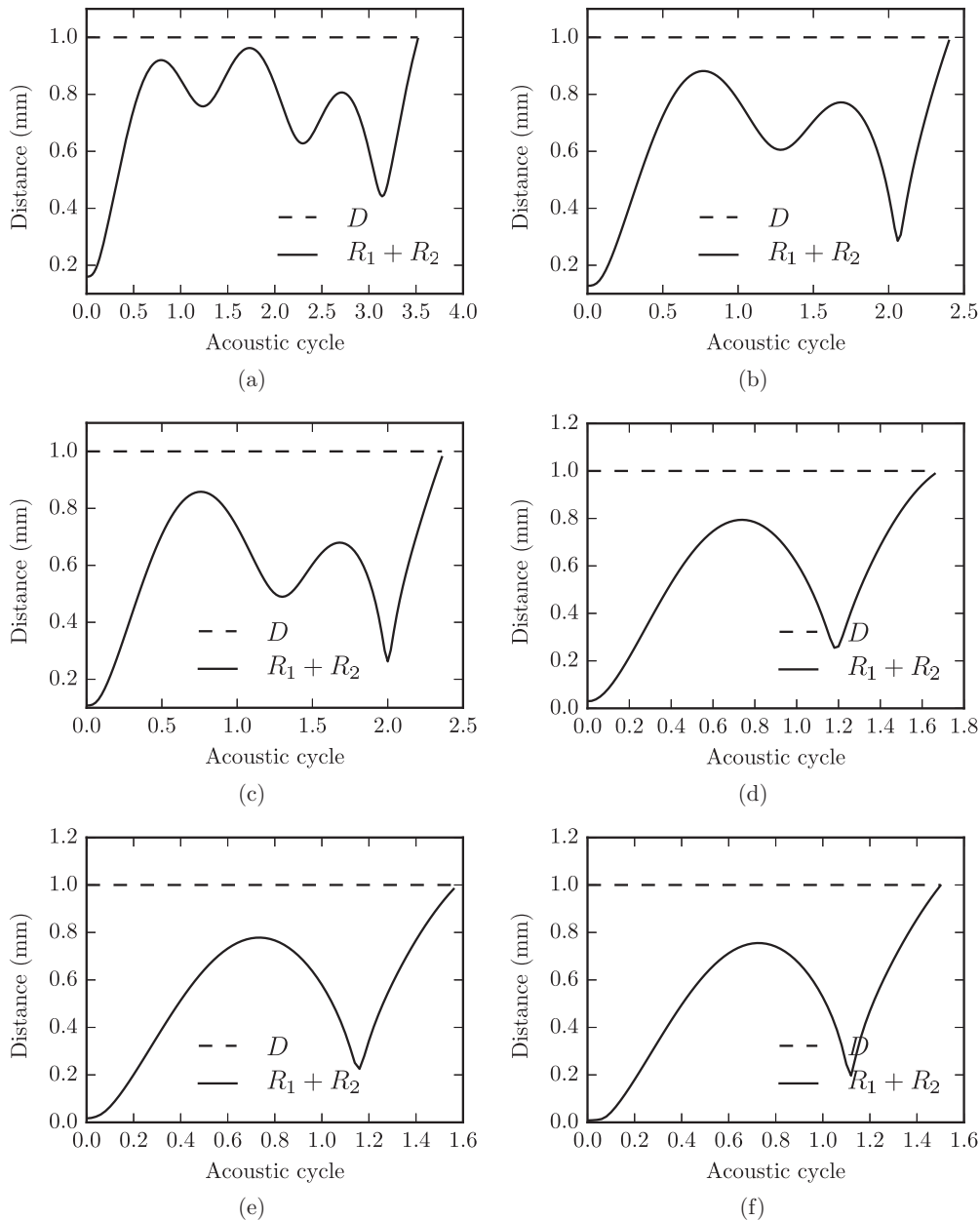
FIG. 5. Sum of instantaneous bubble radii and distance between bubbles for $P_a = 1.0$ MPa, $f = 17.7$ kHz, and $D(t = 0) = 1$ mm. (a) $R_{10} = R_{20} = 80$ μm; $f_{10} = f_{20} = 8.9$ kHz. (b) $R_{10} = R_{20} = 64$ μm; $f_{10} = f_{20} = 17.7$ kHz. (c) $R_{10} = R_{20} = 54$ μm; $f_{10} = f_{20} = 26.6$ kHz. (d) $R_{10} = R_{20} = 15$ μm; $f_{10} = f_{20} = 200$ kHz. (e) $R_{10} = R_{20} = 8.4$ μm; $f_{10} = f_{20} = 400$ kHz. (f) $R_{10} = R_{20} = 4.1$ μm; $f_{10} = f_{20} = 1.04$ MHz.

either for degassing or for grain-refining applications. It is also evident that not only the forcing frequency is important in designing a system, but also its various harmonics, which can be defined by the crucible geometry, and that are likely to resonate with particular bubble sizes.

The pressure that is felt at a distance $D(t = 0)$ away from the bubble center and the associated Fourier transforms are shown in Fig. 7. Large values of pressures, of the order of MPa, are registered a few millimeters away from the cavitating bubbles. These shock waves are a possible cause for the disruption of the growth of the solidification front (including the rupture of secondary dendrite arms [14]) and the random occurrence of cavitation implosions contributing to the grain refining process of the treated melt, in addition to the dominant

effect of the cavitation-induced multiplication of nucleation sites [1]. Each pressure signal attributed to unstable cavitating bubbles contains a strong component of the forcing frequency (17.7 kHz) and only minute traces of harmonics and broadband noise. Cavitometers registering signals at the megahertz range are, therefore, listening to bubbles that are immediately close to their immersed surface.

Figures 7(a), 7(c), and 7(e) show that bubbles of initial radii 80, 64, and 54 μm emit very large pressures, larger than 5.0 MPa. These radii correspond to the forcing frequency and sub- and ultraharmonics, for which large amplitudes were recorded by the cavitometer [Fig. 4(a)]. At these large separations, bubble oscillations are not damped by the interactions with their neighbors, leading to large emitted pressures locally.
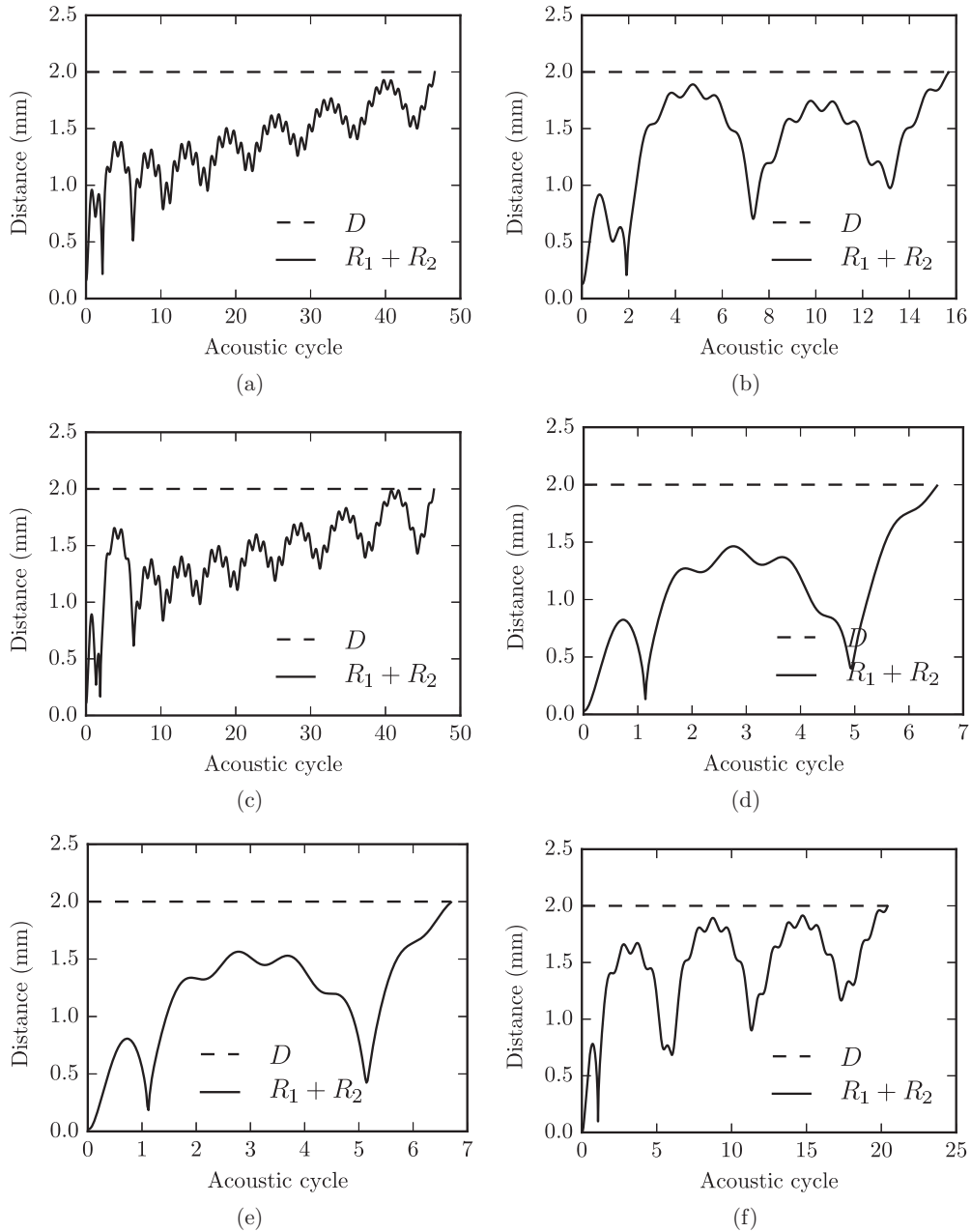
FIG. 6. Sum of instantaneous bubble radii and distance between bubbles for $P_a = 1.0$ MPa, $f = 17.7$ kHz, and $D(t = 0) = 2$ mm. (a) $R_{10} = R_{20} = 80$ μm; $f_{10} = f_{20} = 8.9$ kHz. (b) $R_{10} = R_{20} = 64$ μm; $f_{10} = f_{20} = 17.7$ kHz. (c) $R_{10} = R_{20} = 54$ μm; $f_{10} = f_{20} = 26.6$ kHz. (d) $R_{10} = R_{20} = 15$ μm; $f_{10} = f_{20} = 200$ kHz. (e) $R_{10} = R_{20} = 8.4$ μm; $f_{10} = f_{20} = 400$ kHz. (f) $R_{10} = R_{20} = 4.1$ μm; $f_{10} = f_{20} = 1.04$ MHz.

This phenomenon is very promising for generating strong local velocity jets that can deagglomerate clusters of nanoparticles or break dendrites to enhance columnar to equiaxial growth transition; both of these effects lead to a finer grain structure, which is a desired trait for solidified metals and alloys [1].

melt, particularly for frequencies lower than 22 kHz; these frequency values are favorable for degassing aluminium melt. The large values of the emitted acoustic pressures from isolated bubbles that resonate with the forcing frequency are likely to promote grain refinement by disrupting the growth of the solidification front.

IV. CONCLUSIONS

In this paper, a model from the literature has been extended and applied to determine the dynamics of two interacting hydrogen bubbles subjected to a strong acoustic field in liquid aluminum. The results show that large forcing signals of the order of 1.0 MPa lead to fast coalescence within the
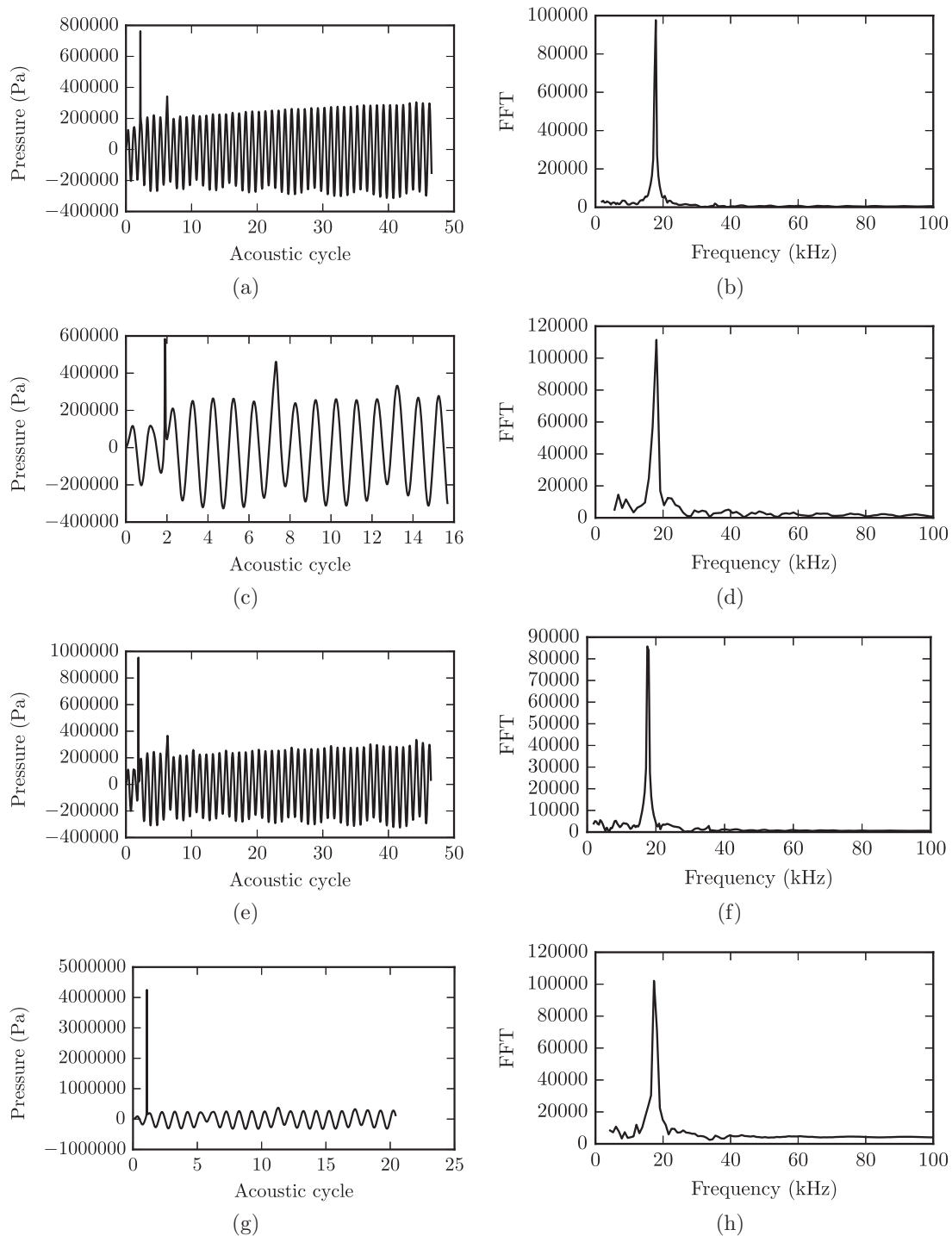
FIG. 7. Emitted pressure at initial separation (left column) and associated fast Fourier transform (right column) for $P_a = 1.0$ MPa, $f = 17.7$ kHz, and $D(t = 0) = 2$ mm. (a), (b) $R_{10} = 80$ μm. (c), (d) $R_{10} = 64$ μm. (e), (f) $R_{10} = 54$ μm. (g), (h) $R_{10} = 4.1$ μm.

[1] G. I. Eskin and D. G. Eskin, *Ultrasonic Treatment of Light Alloy Melts*, 2nd ed. (CRC Press, Boca Raton, FL, 2014).

[2] J. Campbell, Int. Metals Rev. **26**, 71 (1981).

[3] G. Cao, H. Konishi, and X. Li, Mater. Sci. Eng. A **486**, 357 (2008).

[4] N. Alba-Baena and D. Eskin, in *Light Metals 2013* (John Wiley & Sons, Inc., New York, 2013), pp. 957–962.

[5] G. I. Eskin, G. S. Makarov, and Y. P. Pimenov, Adv. Performance Materials **2**, 43 (1995).

[6] G. I. Eskin, Ultrasonics Sonochem. **2**, S137 (1995).

[7] S. Komarov, K. Oda, Y. Ishiwata, and N. Dezhkunov, Ultrasonics Sonochem. **20**, 754 (2013).

[8] L. Nastac, Metal. Materials Trans. B **42**, 1297 (2011).

[9] G. S. B. Lebon, K. Pericleous, I. Tzanakis, and D. G. Eskin, IOP Conf. Ser.: Mater. Sci. Eng. **72**, 052050 (2015).

[10] G. S. B. Lebon, K. Pericleous, I. Tzanakis, and D. G. Eskin, in *Advances in the Science and Engineering of Casting Solidification: An MPMD Symposium Honoring Doru Michael Stefanescu*, edited by L. Nastac, B. Liu, H. Fredriksson, J. Lacaze, C.-P. Hong, A. V. Catalina, A. Buhrig-Polaczek, C. Monroe, A. S. Sabau, R. E. L. Ruxanda, A. Luo, S. Sen, and A. Diószegi (John Wiley & Sons, Inc., Hoboken, NJ, USA, 2015), pp. 23–30.

[11] V. F. K. Bjerknes, *Fields of Force* (Columbia University Press, New York, 1906).

[12] W. Xu, I. Tzanakis, P. Srirangam, S. Terzi, W. Mirihanage, D. Eskin, R. Mathiesen, A. Horsfield, and P. Lee, in *TMS2015 Supplemental Proceedings* (John Wiley & Sons, Inc., New York, 2015), pp. 61–66.

[13] H. Huang, D. Shu, Y. Fu, J. Wang, and B. Sun, Ultrasonics Sonochem. **21**, 1275 (2014).

[14] J. Mi, D. Tan, and T. Lee, Metal. Mater. Trans. B **46**, 1615 (2015).

[15] C.-D. Ohl, T. Kurz, R. Geisler, O. Lindau, and W. Lauterborn, Philos. Trans. R. Soc. London A: Math. Phys. Eng. Sci. **357**, 269 (1999).

[16] S. Luther, R. Mettin, P. Koch, and W. Lauterborn, Ultrasonics Sonochem. **8**, 159 (2001).

[17] R. Mettin, I. Akhatov, U. Parlitz, C. D. Ohl, and W. Lauterborn, Phys. Rev. E **56**, 2924 (1997).

[18] N. A. Pelekasis, A. Gaki, A. Doinikov, and J. A. Tsamopoulos, J. Fluid Mech. **500**, 313 (2004).

[19] L. Jiang, F. Liu, H. Chen, J. Wang, and D. Chen, Phys. Rev. E **85**, 036312 (2012).

[20] A. A. Doinikov, Phys. Rev. E **64**, 026301 (2001).

[21] O. Kapustina, in *Physical Principles of Ultrasonic Technology*, Part IV (Plenum Press, USA, 1973), pp. 422–427.

[22] J. J. Jasper, J. Phys. Chem. Ref. Data **1**, 841 (1972).

[23] Y.-J. Chen, W.-N. Hsu, and J.-R. Shih, Mater. Trans. **50**, 401 (2009).

[24] J. B. Keller and M. Miksis, J. Acoust. Soc. Am. **68**, 628 (1980).

[25] A. Prosperetti, J. Acoust. Soc. Am. **61**, 17 (1977).

[26] Y. Zhang, Int. Commun. Heat Mass Transfer **43**, 1 (2013).

[27] V. G. Levich, *Physicochemical Hydrodynamics* (Prentice-Hall, Englewood Cliffs, NJ, 1962).

[28] M. Minnaert, Philos. Mag. **16**, 235 (1933).

[29] I. Tzanakis, G. S. B. Lebon, D. G. Eskin, and K. Pericleous, Trans. Indian Inst. Met. (2015).

[30] M. Hodnett, and I. Tzanakis, Calibration and characterisation of high-temperature cavitometer, National Physical Laboratory (Ref. No.: 2013030011), London, UK (2014).

[31] Wolfram Research, Inc., *Mathematica 10.1* (2015).

[32] M. M. van Iersel, N. E. Benes, and J. T. Keurentjes, Ultrasonics Sonochem. **15**, 294 (2008).

[33] I. Pelicella, Dodotronic Ultramic Ultrasonic USB Microphones User Guide, Dodotronic (2014).